https://doi.org/10.5194/wes-2021-45
Preprint. Discussion started: 21 May 2021

eawe european academy of wind energy
Open Access WIND ENERGY SCIENCE DISCUSSIONS

2D Numerical Simulation Study of Airfoil Performance

Nasser Shelil

Mechanical Engineering Department, College of Applied Engineering, King Saud University, S.A. & Port Said University, Egypt

Correspondence to: Nasser Shelil (nshelil@ksu.edu.sa)

Abstract. The aerodynamic characteristics of DTU-LN221 airfoil is studied. ANSYS Fluent is used to simulate the airfoil performance with seven different turbulence models. The simulation results for the airfoil with different turbulence models are compared with the wind tunnel experimental data performed under the same operating conditions. It is found that there is a good *agreement* between the computational fluid dynamics (CFD) predicted aerodynamic force coefficients with wind tunnel experimental data especially with angle of attack between -5° to 10°. RSM is chosen to investigate the flow field structure and the surface pressure coefficients under different angle of attack between -5° to 10°. Also the effect of changing air temperature, velocity and turbulence intensity on lift and drag coefficients/forces are examined. The results show that it is recommended to operate the wind turbines airfoil at low air temperature and high velocity to enhance the performance of the wind turbines.

Keywords. Airfoil – Wind Turbine – CFD – Turbulence Models – Simulation – Aerodynamic Performance – Lift and Drag.

1 Introduction

The trend of using renewable energy resources has increases significantly during the past decade. The ~~using~~ of wind power is a promising power generation technology that can help the world to eliminate the dependency on the fuel based sources such as oil and gas. It also helps the environment to be flourished without greenhouse effects or other pollutants. The wind turbine technology offers electrical energy with lower installation and maintenance costs ~~unlike the~~ other energy sources. It is clean, eco-friendly and prime national security at a time when the decreasing global reserves of fossil fuels is an eminent danger in the sustainability of global economy (N. Karthikeyan, 2015).

~~Airfoil~~ is a basic element of a wind turbine blade, and its aerodynamic characteristics have a major influence on the wind energy conversion efficiency. ~~Airfoil~~ is the cross section of a wind turbine blade ~~which~~ is used to generate mechanical force due to the motion of air around the airfoil. The design of wind turbine airfoils is a basic but important task for designing optimal wind turbine rotors. Different types of airfoils are used along the blades in order to generate energy from the wind. The pressure differences in the airfoil cause a force with two main components:

Lift force: it the component of force that acts ~~on the vertical direction of~~ oncoming airflow. It is a result of the unequal pressure on the upper and lower airfoil surfaces. It is given by:

$$F_L = C_L (½\rho A V^2) \quad (1)$$

Where C_L is the lift force coefficient ρ is the density of air, A is the projected airfoil area (Chord x span), V is the velocity of the undistributed air flow and ($½\rho A V^2$) is the dynamic force

Drag Force: it the component of force that acts in the ~~parallel direction of~~ oncoming airflow. It is a result of both viscous friction forces at the surface of the airfoil and the unequal pressure on the upper and lower airfoil surfaces. It is given by:

$$F_D = C_D (½\rho A V^2) \quad (2)$$

Where C_D is the drag force coefficient and ($½\rho A V^2$) is the dynamic force

Lift and drag forces on an airfoil are influenced by the angle of attack, AOA, which is the angle between the distributed wind direction and the chord of the airfoil (Namiranian, 2011). In order to get more performance from the rotor, it is required to maximize the lift force and minimize the drag ~~force.by optimize~~ the angle of attack to obtain the best performance.

https://doi.org/10.5194/wes-2021-45
Preprint. Discussion started: 21 May 2021

eawe european academy of wind energy
Open Access WIND ENERGY SCIENCE DISCUSSIONS

Junwei Yang et al., (Yang et al., 2020) investigate experimentally the effect of turbulent flow on an airfoil with a Gurney flap. The wind tunnel experiments were performed for the DTU-LN221 airfoil under different turbulence level. The results demonstrate that under low turbulent inflow condition, the maximum lift coefficient of the airfoil with flaps increased by 8.47% to 13.50% (i.e., thickness of 0.75%), and the Gurney flap became less effective after stall angle. Other studies are performed to ~~Study of~~ a Gurney ~~F~~lap implementation both experimentally and numerically using RANS based numerical simulations (Iñigo Aramendia 2019).

The different turbulence models have significant impacts on the aerodynamic performance of wind turbine blade airfoil. The numerical simulation method ~~of investigation~~ the behavior of flow around the airfoil has a strong adaptability of time-saving, low cost, easy to reveal the details of the flow field, compared ~~with~~ wind tunnel experiment.

H. Wang et. al., (Hao Wang, ~~Augest~~, 2014) compared the aerodynamic simulation results with the theoretical values of the lift coefficients, drag coefficients and the ratio of lift coefficient to drag ~~coefficient for~~ the forecast of best angle of attack, the effects of these three turbulence models on the blade airfoil aerodynamic performance were estimated. They used three different turbulence models which are S-A, k-εRNG, k-ωSST ~~on~~ the aerodynamic performance of wind turbine airfoil under different ~~attack angles~~. Their simulation results demonstrate that, for the selected blade airfoil, using S-A turbulence model before the best attack angle and k-εRNG turbulence model after the best attack angle respectively.

Two dimensional airfoil's aerodynamic performance was simulated numerically by Ji Yaoa et al. (Ji Yaoa, 2012). The ~~control~~ equations were Navier-Stokes equations, and four turbulence models were applied: Standard k-ε model of two equations, RNG k-ε model, ~~Transition~~ SST model of four equations and Reynolds stress model of five equations. The lift coefficient curves of four turbulence models were much closer ~~with~~ the experimental data, while drag coefficient curves differed largely ~~with~~ the experimental data. This may be caused by the roughness of front edge or other factors. ~~Five~~ equations Reynolds stress model ~~had~~ best result ~~in~~ four turbulence models.

Aftab et al., (S. M. A. Aftab, 2016) studied the Low Reynolds Number flows over airfoil. The turbulence models tested were: one equation Spallart Allmars (S-A), two equation SST K-ω, three equation Intermittency (γ) SST, k-kl-ω and finally, the four equation transition γ-Reθ SST. The results obtained show the values of the experimental study and the current CFD study are found to be in good agreement. This Study clearly shows that capturing the transition behaviour, for low Reynolds numbers flows, needs an accurate turbulence model. In the present case, γ-Reθ SST is preferred model as it predicts the flow behaviour both at low and high AoA, accurately and in a short duration of time.

Unsteady aerodynamic characteristics is studied by G. H. Yu et.al. (G. H. Yu, 2010). They used ~~using~~ two-dimensional CFD with Menter's transition corrected K−ω SST turbulence model for various reduced frequencies. They observed that flow separation is delayed to higher angles of attack compared ~~with~~ the static stall case, and the lift force is found to increase far beyond that ~~at~~ the static stall angle. Reduced frequency is observed to have a significant impact on the aerodynamic forces and the pitching moment. The peak in the lift force coefficient appears at a higher angle of attack with increasing reduced frequency.

The turbulence model has a definitely great influence on the numerical simulation results of wind turbine blade airfoil. Traditional numerical simulation process did not consider the impacts of the changed angle of attack on the simulation results, no matter how much the angle of attack is, only one single kind of turbulence model was applied to simulate the aerodynamic performance of wind turbine blade airfoil. This simulation method for airfoil aerodynamic performance has a large error result (Hao Wang, ~~Augest~~, 2014).

This work aims to simulate the behavior and performance of airfoil under different working conditions. A 2D model is considered in Ansys Fluent CFD simulation of DTU-LN221 airfoil. Seven different turbulence models are used to perform the simulation. The simulation results are compared ~~with~~ the experimental data to choose the suitable turbulence model to continu~~ing~~ the investigation of the flow characteristics over the airfoil. The effect of the angle of attack ~~of~~ lift and drag

https://doi.org/10.5194/wes-2021-45
Preprint. Discussion started: 21 May 2021

eawe european academy of wind energy
Open Access WIND ENERGY SCIENCE DISCUSSIONS

coefficients is investigated. The pressure coefficient is monitored at different angles of attack. The effect of temperature, air velocity and turbulence intensity on the airfoil performance is demonstrated.

2 Methodology

2.1 Physical Model

The DTU-LN221 airfoil have been designed according to the requirements provided by LM and tested in the LM wind tunnel (2015a; Cheng et al., 2014). The design of such type of wind turbine rotors have aerodynamically high efficiency, low cost and low noise emission (Jt Cheng, 2014).

The DTU-LN221 airfoil model (Cheng, 2013; Sessarego, 2016; Yang et al., 2020; 2015a), as shown in Figure 1, was adopted which has a chord length of 0.6 m and a span ~~length~~ of 1.5 m. The airfoil model was vertically placed in the test section. The bottom part of the airfoil section was connected by the rotating shaft, which was fixed on a rotational plate. Therefore, the angle of attack can be remotely controlled via a shaft connection with a motor below the wind tunnel. The airfoil model was made of aluminum alloy.

In the experiment, the free stream flow velocity was 37.5 m/s, and the corresponding Reynolds number based on the airfoil chord length was 1.5 x 10^6, although wind turbines often operate at wind speed below 37.5 m/s, but the magnitude of the Reynolds number was up to an order of 10^6. Therefore, the experimental value of the Reynolds number was chosen to approach an order of magnitude corresponding to those obtained from full-scale wind turbines (Yang et al., 2020; Roha. ~~Lswt Campaign Report on Dtu C21; Lm Internal Report: Jupitervej~~).

The full description of the design of the airfoil profile is ~~described~~ in details in (Sessarego, 2016; Yang et al., 2020).

Table 1 show the basic data for the airfoil and operating conditions of the experimental data (Sessarego, 2016; Yang et al., 2020).

Table 1: Basic data chosen for wind-turbine airfoil model

Property	Value
Airfoil name	DTU-LN221
Density of air	1.205 kg/m^3
Dynamic viscosity of air	1.821 x 10^5 Ns/m^2
Air Temperature	293 K
Design wind speed, Vo	37.5 m/s
Re	1.5 x 10^6
Airfoil chord	0.600 m
Airfoil thickness relative to chord	21%
Airfoil length	1.5 m
Material	aluminum alloy

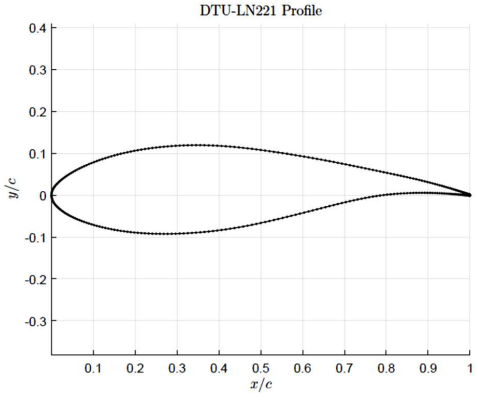

Figure 1: ~~Profile~~ coordinates of the DTU-LN221 airfoil (Sessarego, 2016)

https://doi.org/10.5194/wes-2021-45
Preprint. Discussion started: 21 May 2021

eawe european academy of wind energy
Open Access WIND ENERGY SCIENCE DISCUSSIONS

2.2 Mathematical Modeling (Turbulence Models)

2.2.1 Inviscid flow

Inviscid flow analyses neglect the effect of viscosity on the flow and are appropriate for high-Reynolds-number applications where inertial forces tend to dominate viscous forces. The inviscid is appropriate flow calculations of high-speed aerodynamic analysis as the pressure forces on the body will dominate the viscous forces. Hence, an inviscid analysis will give you a quick estimate of the primary forces acting on the body. After the body shape has been modified to maximize the lift forces and minimize the drag forces, you can perform a viscous analysis to include the effects of the fluid viscosity and turbulent viscosity on the lift and drag forces.

For inviscid flows, ANSYS Fluent solves the Euler equations. The mass conservation equation is the same as for a laminar flow, but the momentum and energy conservation equations are reduced due to the absence of molecular diffusion.

- *The Mass Conservation Equation:*

The equation for conservation of mass, or continuity equation, can be written as follows:

$$\frac{\partial \rho}{\partial t} + \nabla.(\rho \vec{v}) = S_m \tag{3}$$

The source S_m is the mass added to the continuous phase from the dispersed second and any user-defined sources.

- *Momentum Conservation Equations:*

Conservation of momentum is described by:

$$\frac{\partial}{\partial t}(\rho \vec{v}) + \nabla.(\rho \vec{v}\vec{v}) = -\nabla p + \rho \vec{g} + \vec{F} \tag{4}$$

where p is the static pressure and ρg and F are the gravitational body force and external body forces respectively. F also contains other model-dependent source terms such as porous-media and user-defined sources.

- *Energy Conservation Equation:*

Conservation of energy is described by:

$$\frac{\partial}{\partial t}(\rho E) + \nabla.(\vec{v}.(\rho E + p)) = -\nabla.\left(\sum_j h_j J_j\right) + S_h \tag{5}$$

2.2.2 Reynolds Average Navier Stoke(RANS)

In CFD, RANS is the most widely used turbulence modelling approach. In this approach, the Navier Stokes equations are split into mean and fluctuating components. The total velocity u_i is a function of the mean velocity $\bar{u}_i$ and the fluctuating velocity $\acute{u}_i$ as shown in the equation below (Hinze, 1975).

$$u_i = \bar{u}_i + \acute{u}_i \tag{6}$$

The continuity and momentum equation incorporating these instantaneous flow variables are given by:

$$\frac{\partial \rho}{\partial t} + \frac{\partial}{\partial x_i}(\rho u_i) = 0 \tag{7}$$

$$\frac{\partial}{\partial t}\rho u_i + \frac{\partial}{\partial x_i}(\rho u_i u_j) = \frac{\partial \rho}{\partial x_i} + \frac{\partial}{\partial x_j}\left[\mu\left(\frac{\partial u_i}{\partial x_j} + \frac{\partial u_j}{\partial x_i} - \frac{2}{3}\delta_{ij}\frac{\partial u_i}{\partial x_i}\right)\right] + \frac{\partial}{\partial x_i}(-\rho\overline{\acute{u}_i\acute{u}_j}) \tag{8}$$

These above equations (in Cartesian tensor form) are known as RANS equations, and the additional Reynolds stress terms $-\rho\overline{\acute{u}_i\acute{u}_j}$ need to be modelled. The Boussinesq hypothesis is applied in relating the Reynolds stress and mean velocity:

$$-\rho\overline{\acute{u}_i\acute{u}_j} = \mu_t\left(\frac{\partial u_i}{\partial x_j} + \frac{\partial u_j}{\partial x_i}\right) - \frac{2}{3}\left(\rho k + \mu_t\frac{\partial u_{ik}}{\partial x_k}\right)\delta_{ij} \tag{9}$$

2.2.3 Spallart Allmars (S-A)

The S-A turbulence model is a one-equation model, designed for aerospace applications. It is quite robust and effective in modelling the flow on an airfoil, with adverse pressure gradients in the boundary layer (Allmaras, 1992; W., 2007). The modified continuity equation for S-A solves the turbulent viscosity $\tilde{v}$.

https://doi.org/10.5194/wes-2021-45
Preprint. Discussion started: 21 May 2021

eawe european academy of wind energy
Open Access WIND ENERGY SCIENCE DISCUSSIONS

$$\frac{\partial}{\partial t}\rho\tilde{v} + \frac{\partial}{\partial x_i}(\rho\tilde{v}u_i) = G_v = \frac{1}{\sigma\tilde{v}}\left[\frac{\partial}{\partial x_j}\left\{(\mu + \rho\tilde{v})\frac{\partial\tilde{v}}{\partial x_j}\right\} + C_{b2\rho}\left(\frac{\partial\tilde{v}}{\partial x_j}\right)^2\right] - Y_v + S\tilde{v} \quad (10)$$

G_v is the production of turbulent viscosity and Y_v is the destruction of turbulent viscosity.

The turbulent viscosity is calculated as shown

$$\mu_t = \rho\tilde{v}f_{v1} \quad (11)$$

The f_{v1} is the viscous damping function

$$f_{v1} = \frac{\chi^3}{\chi^3 + C_{v1}^3} \quad (12)$$

It has been reported that this model is effective for low Reynolds number cases, provided that the mesh resolution is super fine with a wall $Y^+ \leq 1$ (2015b; 2015c).

2.2.4 Standard k-ε Model

Two-equation turbulence models allow the determination of both, a turbulent length and time scale by solving two separate transport equations. The standard - model in ANSYS Fluent falls within this class of models and has become the workhorse of practical engineering flow calculations in the time since it was proposed by Launder and Spalding (Spalding, 1972). Robustness, economy, and reasonable accuracy for a wide range of turbulent flows explain its popularity in industrial flow and heat transfer simulations. It is a semi-empirical model, and the derivation of the model equations relies on phenomenological considerations and empiricism.

The standard k-ε model (Spalding, 1972) is a model based on model transport equations for the turbulence kinetic energy (k) and its dissipation rate (ε). The model transport equation for k is derived from the exact equation, while the model transport equation for ε was obtained using physical reasoning and bears little resemblance to its mathematically exact counterpart.

In the derivation of the k-ε model, the assumption is that the flow is fully turbulent, and the effects of molecular viscosity are negligible. The standard k-ε model is therefore valid only for fully turbulent flows.

The turbulence kinetic energy, k, and its rate of dissipation, ε, are obtained from the following transport equations:

$$\frac{\partial}{\partial t}(\rho k) + \frac{\partial}{\partial X_i}(\rho k u_i) = \frac{\partial}{\partial x_j}\left[\left(\mu + \frac{\mu_t}{\sigma_k}\right)\frac{\partial k}{\partial x_j}\right] + G_k + G_b - \rho\varepsilon - Y_M + S_k \quad (13)$$

And

$$\frac{\partial}{\partial t}(\rho\varepsilon) + \frac{\partial}{\partial X_i}(\rho\varepsilon u_i) = \frac{\partial}{\partial x_j}\left[\left(\mu + \frac{\mu_t}{\sigma_\epsilon}\right)\frac{\partial\varepsilon}{\partial x_j}\right] + C_{1\varepsilon}\frac{\varepsilon}{k}(G_k + C_{3\varepsilon}G_b) - C_{2\epsilon}\rho\frac{\varepsilon^2}{k} + S_\varepsilon \quad (14)$$

Where G_k represents the generation of turbulence kinetic energy due to the mean velocity gradients, G_b is the generation of turbulence kinetic energy due to buoyancy, Y_M represents the contribution of the fluctuating dilatation in compressible turbulence to the overall dissipation rate, $C_{1\varepsilon}$, $C_{2\varepsilon}$, and $C_{3\varepsilon}$ are constants. σ_k and σ_ε are the turbulent Prandtl numbers for k and ε, respectively. S_k and S_ε are user-defined source terms.

The turbulent viscosity, μ_t, is computed by combining k and ε as follows:

$$\mu_t = \rho C_\mu \frac{k^2}{\epsilon} \quad (15)$$

Where C_μ is a constant.

The default values of the model constants are (Spalding, 1972):

$C_{1\varepsilon}$=1.44, $C_{2\varepsilon}$=1.92, C_μ=0.09, σ_k=1.0 and σ_ε=1.3

2.2.5 The RNG - model

The RNG - model was derived using a statistical technique called renormalization group theory. It is similar in form to the standard k-ε model, but includes the following refinements:

- The RNG model has an additional term in its equation that improves the accuracy for rapidly strained flows.

https://doi.org/10.5194/wes-2021-45
Preprint. Discussion started: 21 May 2021

eawe european academy of wind energy
Open Access WIND ENERGY SCIENCE DISCUSSIONS

- The effect of swirl on turbulence is included in the RNG model, enhancing accuracy for swirling flows.
- The RNG theory provides an analytical formula for turbulent Prandtl numbers, while the standard k-ε model uses user-specified, constant values.
- While the standard k-ε model is a high-Reynolds number model, the RNG theory provides an analytically-derived differential formula for effective viscosity that accounts for low-Reynolds number effects. Effective use of this feature does, however, depend on an appropriate treatment of the near-wall region.

These features make the RNG k-ε model more accurate and reliable for a wider class of flows than the standard k-ε model.

The RNG-based k-ε turbulence model is derived from the instantaneous Navier-Stokes equations, using a mathematical technique called "renormalization group" (RNG) methods. The analytical derivation results in a model with constants different from those in the standard k-ε model, and additional terms and functions in the transport equations for k and ε. A more comprehensive description of RNG theory and its application to turbulence can be found in (S. A. Orszag, 1993).

2.2.6 Standard k-ω Model

The standard k-ω model in ANSYS Fluent is based on the Wilcox k-ω model (Wilcox, 1998), which incorporates modifications for low-Reynolds number effects, compressibility, and shear flow spreading. One of the weak points of the Wilcox model is the sensitivity of the solutions to values for k and ω outside the shear layer (freestream sensitivity). While the new formulation implemented in ANSYS Fluent has reduced this dependency, it can still have a significant effect on the solution, especially for free shear flows (Menter, 2009).

The standard k-ω model is an empirical model based on model transport equations for the turbulence kinetic energy (k) and the specific dissipation rate (ω), which can also be thought of as the ratio of ω to k (Wilcox, 1998).

As the k-ω model has been modified over the years, production terms have been added to both the k and ω equations, which have improved the accuracy of the model for predicting free shear flows.

The turbulence kinetic energy, k, and the specific dissipation rate, ω, are obtained from the following transport equations:

$$\frac{\partial}{\partial t}(\rho k) + \frac{\partial}{\partial x_i}(\rho k u_i) = \frac{\partial}{\partial x_j}\left[\Gamma_k \frac{\partial k}{\partial x_j}\right] + G_k - Y_k + S_k \quad (16)$$

And

$$\frac{\partial}{\partial t}(\rho \omega) + \frac{\partial}{\partial x_i}(\rho \omega u_i) = \frac{\partial}{\partial x_j}\left[\Gamma_\omega \frac{\partial \omega}{\partial x_j}\right] + C_\omega - Y_\omega + S_\omega \quad (17)$$

Where G_k represents the generation of turbulence kinetic energy due to mean velocity gradients. G_ω represents the generation of ω. Γ_k and Γ_ω represent the effective diffusivity of k and ω, respectively. Y_k and Y_ω represent the dissipation of k and ω due to turbulence. All of the above terms are calculated as described below. S_k and S_ω are user-defined source terms.

2.2.7 Shear-Stress Transport (SST) k-ω model

The shear-stress transport (SST) k-ω model was developed by Menter (Menter, 1994). It is a combination of the Wilcox K-ω and the standard K-ε model. It is so named because the definition of the turbulent viscosity is modified to account for the transport of the principal turbulent shear stress. The standard K-ε is transformed to K-ω by substituting ε = Kω (W., 2007). It has feature that gives the SST k-ω model an advantage in terms of performance over both the standard k-ω model and the standard k-ε model. Other modifications include the addition of a cross-diffusion term in the ω equation and a blending function to ensure that the model equations behave appropriately in both the near-wall and far-field zones (2015b; 2015c).

The SST k-ω model has a similar form to the standard k-ω model. The turbulence kinetic energy, k, and the specific dissipation rate, ω, are obtained from the following transport equations:

$$\frac{\partial}{\partial t}(\rho k) + \frac{\partial}{\partial x_i}(\rho k u_i) = \frac{\partial}{\partial x_j}\left(\Gamma_k \frac{\partial k}{\partial x_j}\right) + \tilde{G}_k - Y_k + S_k \quad (18)$$

https://doi.org/10.5194/wes-2021-45
Preprint. Discussion started: 21 May 2021

eawe european academy of wind energy
Open Access WIND ENERGY SCIENCE DISCUSSIONS

and

$$\frac{\partial}{\partial t}(\rho\omega)+\frac{\partial}{\partial x_i}(\rho\omega u_i)=\frac{\partial}{\partial x_j}(\Gamma_\omega\frac{\partial\omega}{\partial x_j})+G_\omega-Y_\omega+D_\omega+S_\omega \quad (19)$$

where

G_k represents the generation of turbulence kinetic energy due to mean velocity gradients. G_ω represents the generation of ω. Γ_k and Γ_ω represent the effective diffusivity of k and ω, respectively. Y_k and Y_ω represent the dissipation of k and ω due to turbulence. D_ω represents the cross-diffusion term. S_k and S_ω are user-defined source terms. Calculations for all previous terms have been fully described in (2015b; 2015c).

2.2.8 The Reynolds stress model (RSM)

The Reynolds stress model (RSM) (B. E. Launder, 1975; Launder, 1989; Launder, 1978) is the most elaborate type of RANS turbulence model that ANSYS Fluent provides. Abandoning the isotropic eddy-viscosity hypothesis, the RSM closes the Reynolds-averaged Navier-Stokes equations by solving transport equations for the Reynolds stresses, together with an equation for the dissipation rate. This means that five additional transport equations are required in 2D flows, in comparison to seven additional transport equations solved in 3D.

Since the RSM accounts for the effects of streamline curvature, swirl, rotation, and rapid changes in strain rate in a more rigorous manner than one-equation and two-equation models, it has greater potential to give accurate predictions for complex flows. However, the fidelity of RSM predictions is still limited by the closure assumptions employed to model various terms in the exact transport equations for the Reynolds stresses. The modeling of the pressure-strain and dissipation-rate terms is particularly challenging, and often considered to be responsible for compromising the accuracy of RSM predictions.

The default Reynolds stress model in ANSYS Fluent is based on the ε-equation, and uses a linear model for the pressure-strain term. The second ε-based model allows the usage of a quadratic model for the pressure-strain term.

The two Reynolds stress models based on the ω-equation both use a linear model for the pressure-strain term, but differ with regard to the scale equation: the stress-omega model is based on the ω-equation, whereas the stress-BSL model solves the scale equation from the baseline (BSL) k-ω model and thus removes the free-stream sensitivity observed with the stress-omega model.

2.3 Numerical Simulation (Model Setup)

Generating the right computational domain for a Fluid Dynamic problem is an important task of the modeling process. It is necessary to take into account different requirements (J., 2015). The domain should not be too small to correctly reproduce the flow around the airfoil and it should not be too large to not uselessly increase cells number of the grid and hence computation time (Rosario Lanzafame). It is preferable to do independency study to select the suitable domain/grid for your case of study. It should to be taken into account the requirements of the meshing in terms of quality and first cell positioning near the airfoil.

3 Results and Discussions

The Ansys R17 package is used to simulate the air flow characteristics over DTULN221 airfoil. The 2-D Design Modeler (DM) is used to draw the airfoil profile by using the coordinates of 300 points to guarantee the smoothness and accuracy of the airfoil profile. The computational domain is composed an upstream C-shape, half of circle, in which the airfoil is included. The airfoil end is located at the center of the semicircle. The diameter of the semicircle is 10 times the chord of the airfoil (Schepers J. G., 2004). The downstream domain is a square with side length equals the circle diameter as shown in Fig. 2. C-H type structured grid is applied in the airfoil domain to consider the boundary layer's effect on the aerodynamic performance

https://doi.org/10.5194/wes-2021-45
Preprint. Discussion started: 21 May 2021

of airfoils. Also considering the requirements of turbulence model ~~for~~ the grid, the boundary layer mesh is denser around the airfoil, so the results met the stability requirements.

The mesh is constructed by Ansys Mesh. 2-D curvature, fine, high smoothing mesh with growth rate of 1.05 is constructed. Different edges and face sizing are chosen to build up different meshes with different number of elements to check the independency of the results.

A mesh dependency study is made to verify that the solution obtained numerically is not dependent on the mesh size. Six different grids were created. ~~All are fine meshes~~ of approximately 108700, 63000, 51000, 36000, 24000 and 16000 cells ~~have~~ been designed, respectively. Both lift and drag dimensionless coefficients were calculated at zero degree angle of attack for the six grids. The grid with 24000 cells generated the same results as the higher number of cells grids. The exact total number of model grid was 23897 elements. It could be seen from the figure that the distribution of the grid was much denser in airfoil's front edge, back edge and airfoils surface. The mesh of the computational domain was shown in Fig 2.a. Airfoil and nearby wall grid were shown in Fig 2.b .

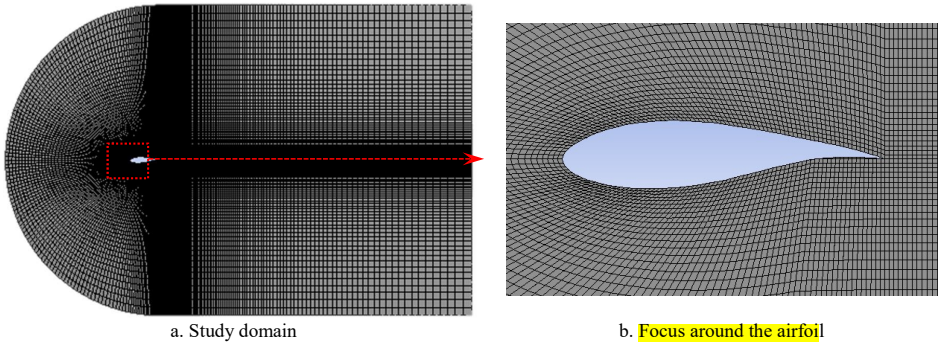

a. Study domain b. Focus around the airfoil

Fig. 2. The integral mesh grid

3.1 Model Validation (Turbulence Models Comparison)

To validate the simulation of the DTULN221 airfoil, seven turbulence models are applied to numerically simulate under the same conditions of Re number, temperature, and turbulence intensity. The air velocity is 37.5 m/s which generates a turbulence with Re of 1.8×10^6. 2D, Double Precession, serial processing options are chosen. Density based, SIMPLE algorithm is used in processing coupling problems of speed and pressure in FLUENT solver. The second-order upwind scheme is used to ~~discrete~~. The Energy Equation is on and Air is considered as a real gas. The initial and boundary conditions are shown in Table 2.

Table 2 : Initial and Boundary Conditions

Boundary Conditions	Type	Variables	notes
inlet	Velocity Inlet	V= 37.5 m/s T= 293 K P_g= 0 kPa T.I. = 0.0011 Turbulent viscosity ratio =10	x and y components of velocity are varied according to AOA
Outlet	Pressure Outlet	T= 293 K P_g= 0 kPa T.I. = 0.0011 Turbulent viscosity ratio =10	
Airfoil surface	Wall	Stationary wall Non slip Zero roughness	
Walls	Wall	Stationary wall	

https://doi.org/10.5194/wes-2021-45
Preprint. Discussion started: 21 May 2021

eawe european academy of wind energy
Open Access WIND ENERGY SCIENCE DISCUSSIONS

		Non slip Zero roughness	
Viscous Model	Alternate: Inviscid, Spalart-Allmaras, k-ε, RNG k-ε, k-ω, SST k-ω and RSM.		
Other Conditions	Air density: ideal gas ~~Air density: ideal gas~~ Airfoil Chord: 0.6 m ~~Airfoil Length = 1.5 m~~ AOA : varied from -10° to 20°		

3.2 Lift and Drag Coefficients

Seven viscous models are used to simulate the flow over DTULN221 airfoil. These models are Inviscid, Spalart-Allmaras, k-ε, RNG k-ε, k-ω, SST k-ω and RSM. The lift and drag coefficients are monitored for each simulation. The results are compared with the experimental findings in (Roha. ~~Lswt Campaign Report on Dtu C21; Lm Internal Report: Jupitervej~~; Yang et al., 2020). Their experimental measured data of the airfoil were corrected by ~~after~~ the reference (Allen, 1944). The experimental values of the lift and drag coefficients of the selected airfoil are compared with the simulated lift and drag coefficients of the seven turbulence models respectively.

Fig. 3 shows the comparison of the lift coefficients simulated by seven turbulent models and the theoretical lift coefficient. In general, Lift force increases with AOA and reaches to the maximum value at an angle of attack of (10°~12°) in this type of airfoil. After this point, the lift coefficient decreases with further increase of AOA due to entering the airflow in turbulent region which separates the boundary layers from the airfoil. Therefore, the drag force rapidly goes up and the lift force goes down ~~at~~ this region.

In order to verify the simulation results of lift coefficients of seven turbulent models, the flow fields given by seven turbulent models are also given subsequently as Fig. 3. According to Fig. 3, the simulated lift coefficients of the theoretical value and seven different turbulence models are very close during the attack angle of -5°: 10° range and more consistent with the experimental values. Lift coefficient increases nearly linearly with the increasing attack angle when the attack angle is smaller than 10°. The lift coefficient results of seven turbulence models show significant differences when the angle of attack is bigger than 10°.

Some reasons of the deviation between the experimental data and the simulation results may be the roughness of the airfoil surface which may affect the experimental results. The pressure of the air fan in the wind tunnel may affect the simulation results as it wasn't taken into consideration. Also, the effect of flow separation may affect the drag force considerably. Airfoil flow separates when airfoil is at a high angle of attack, which is caused by the viscosity of fluid. So, it can be noticed that the inviscid model present a ~~good~~ approximation over the other models at higher angle of attack as it ignores the viscous force.

From Fig. 3, it can be noticed that the results can be divided into three regions:

AOA < -5 in this region there is a noticeable deviation between the experimental results and experiments. Most of the models ~~are~~ approximately gave the same values of lift force but the nearest values with the experiments are given by SST k-ω and RSM.

-5 < AOA < 10 a good results compared with the experimental findings. Both inviscid and RSM show the best approximation while k-ε and Spalart-Allmaras models are the worst.

AOA > 10 a clear diversity of the results appears where the inviscid, k-ω and RSM gave good results with respect to the experimental data. While Spalart-Allmaras model is still the worst.

Fig. 4 shows the comparison of drag coefficient using different viscous models. It is shown that the drag coefficient is small up to AOA<10. Then the drag increases rapidly with the increase of AOA. The best results for drag coefficient are given by the inviscid and RSM models while the worst results are delivered by k-ε model.

https://doi.org/10.5194/wes-2021-45
Preprint. Discussion started: 21 May 2021

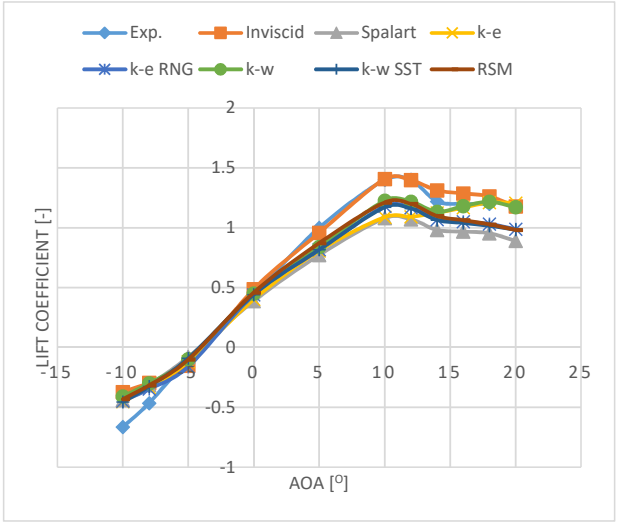

310 Fig. 3 The comparison of lift coefficient using different models

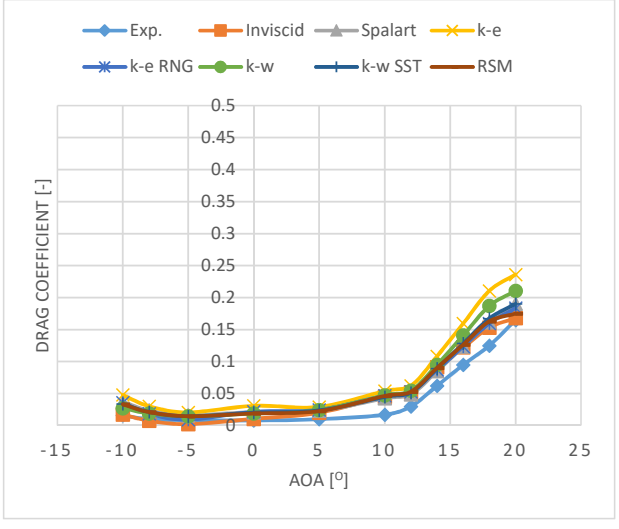

Fig. 4 The comparison of drag coefficient using different models

3.3 Effect of Angle of Attack on the Flow Field

RSM is applied to simulate the fluid field at different angles of attack. Four AOA (-5°, 0°, 5°, and 10°) are chosen to show the
315 flow field represented by pressure and velocity distributions.

Fig. 5 shows the flow fields of wind turbine blade airfoil with different angle of attack. As the AOA increases, ~~T~~the pressure in the lower side of the air foil increases while the velocity decreases. On the other side, upper side, ~~the pressure~~ the pressure is positive with AOA of -5° whereas negative pressure contours emerged in zero and positive AOA. With the decrease of the pressure on the upper side of the airfoil, the velocity increases. ~~The design of such airfoil helps to have extra lift force from~~
320 ~~the tail of the airfoil as well as the front head~~.

The flow field of the trailing edge of wind turbine blade airfoil shows that the flow still belongs to laminar status for the four conditions of AOA, and there are no turbulence and flow separation at all. That is why the simulation results of aerodynamic performance of blade airfoil using this turbulent model is very near and coincide with the experimental values very much.

https://doi.org/10.5194/wes-2021-45
Preprint. Discussion started: 21 May 2021

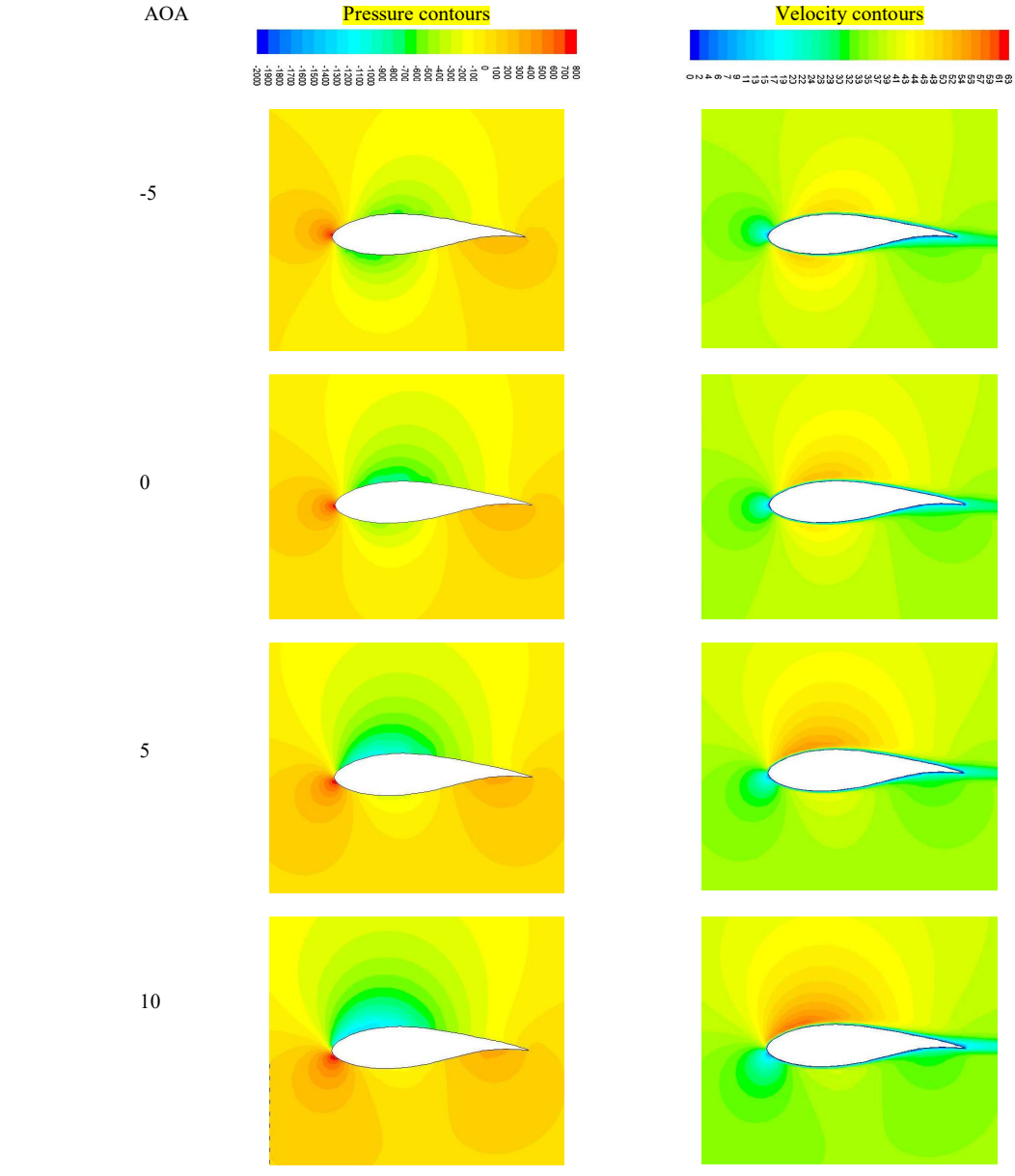

Fig. 5: The flow fields of wind turbine blade airfoil with different angle of attack

3.4 Pressure Coefficient

The pressure coefficient C_p on the airfoil surface is defined as:

$$C_p = \frac{p_i - p_o}{\frac{1}{2}\rho U_o^2}$$

where p_i is the pressure at position i , p_o is the free stream static pressure at the airfoil, ρ is the air density and U_o is the free stream velocity.

The distribution of pressure coefficient of DTULN221 airfoil under different angle of attack is shown in Fig 6. Reynolds stress model (RSM) is applied to perform the simulation. Pressure differences between upper and lower surfaces of the airfoil increases with the AOA increasing. At front edge of airfoil, pressure difference is higher, compared to rear edge, where the lift

https://doi.org/10.5194/wes-2021-45
Preprint. Discussion started: 21 May 2021

is produced. It could be seen from this figure that the airfoil leading edge had a larger curvature, the flow on the airfoil surface would have a large acceleration, then the static pressure would lower on the airfoil's surface. With the increase of the angle of attack, the differences become more larger at the leading edge.

There was an anti-curvature shrinking section on the airfoil rear edge pressure side, which could lower the velocity and increase the pressure as shown also in Fig. 6, so the pressure coefficient of rear edge pressure side had an obvious inclination.

The figure showed that the distribution of pressure on the airfoil's surface varied largely under different attack angle. When the attack angle was less than zero, the pressure coefficient of airfoil's upper surface was positive and lower surface was negative, indicated that at this time lift force of airfoil pointed below. It could be seen from Fig. 6 that the larger attack angle, the greater difference of pressure coefficient between upper and lower surface. For DTULN221 airfoil, the difference of pressure coefficient on the airfoil's front edge was much larger, while on the rear edge was much lower, indicated that the lift force of airfoil mainly come from front edge. For that type of airfoil, when the attack angle was zero, the pressure coefficient of airfoil's upper and lower surface is not equal, as the DTULN221 airfoil is not symmetry. And when the attack angle was larger than zero, the pressure coefficient of airfoil's upper surface was negative and lower surface was positive, indicated that at this time lift force of airfoil pointed up.

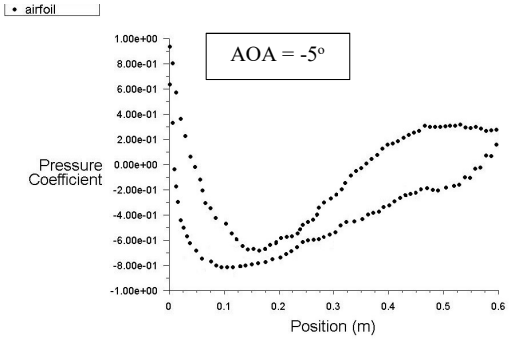

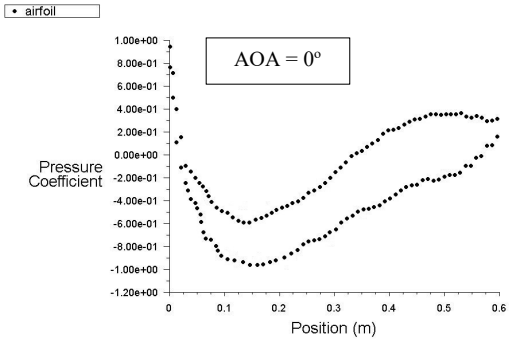

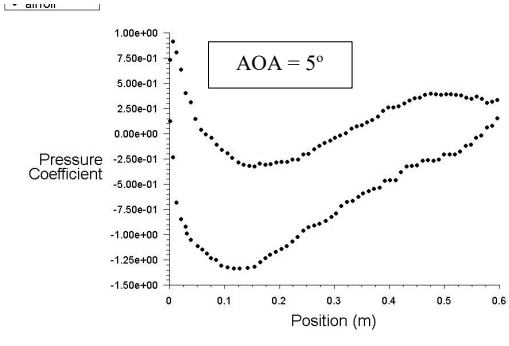

https://doi.org/10.5194/wes-2021-45
Preprint. Discussion started: 21 May 2021

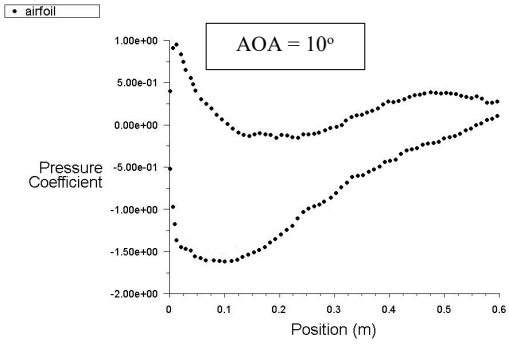

Fig. 6: The surface pressure coefficients under different angle of attack

3.5 Effect of Air Temperature

RSM is used to investigate the effect of changing air temperature on the airfoil characteristics. Both lift and drag coefficients are monitored at different air temperature. The temperature range was from 283 K to 323 K with step 10 K. Air velocity remains constant with a value of 37.5 m/s and turbulence intensity of 0.0011. Fig. 7 shows the comparison of lift coefficient under different air temperature. The lift coefficients are close to each other with a very small variation. Also, there was no noticeable change in the drag coefficients with the variation of air temperature as shown in fig. 8.

Not only lift and drag coefficients are the variables that affect the behavior of the wing turbine but also lift and drag forces. The power delivered from the wind turbine depends on both lift and drag forces. So, it is important to study the effect of other operating variables on lift and drag forces.

Fig. 9 shows the comparison of lift force under different air temperature. The lift force decreases with the increase of air temperature. That is due to the decrease of air density with temperature. It's important to simulate the airfoil with a model that take the variation of the density of air with temperature. The decrease of lift force with temperature tends to a loss in power at high temperature days or high temperature locations which may be taken into considerations in site selection for installing the wind turbine. The loss in the magnitude of the lift force is higher with the increase of AOA.

Fig. 10 shows the comparison of drag force under different air temperature. The drag force decreases with the increase of air temperature.

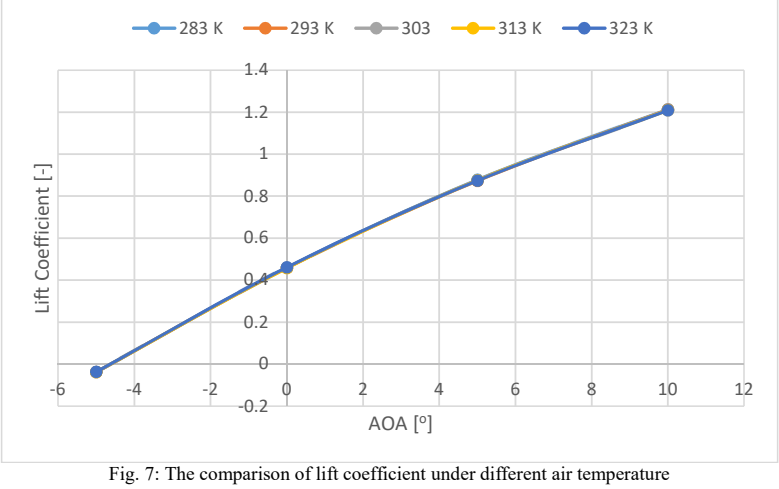

Fig. 7: The comparison of lift coefficient under different air temperature

https://doi.org/10.5194/wes-2021-45
Preprint. Discussion started: 21 May 2021

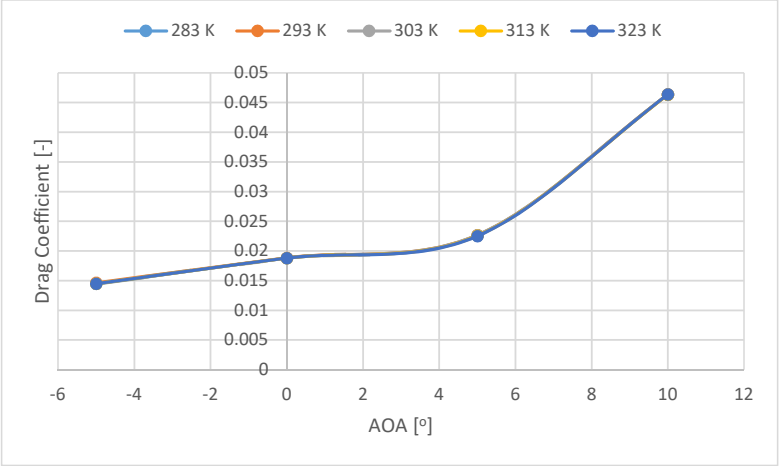

Fig. 8: The comparison of drag coefficient under different air temperature

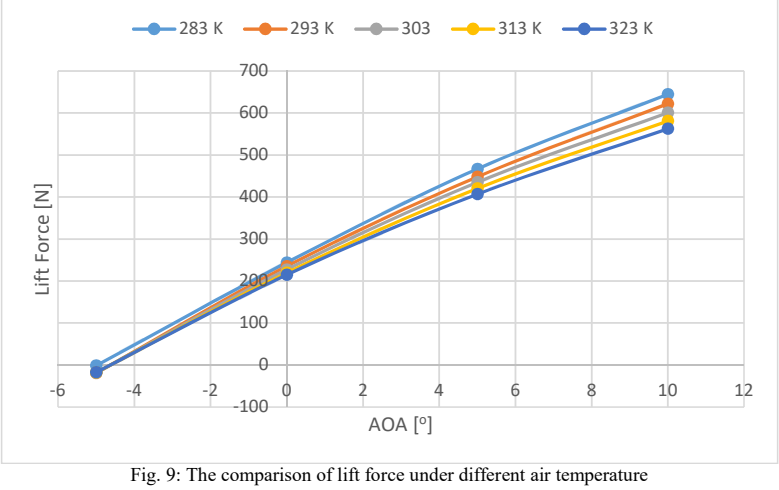

Fig. 9: The comparison of lift force under different air temperature

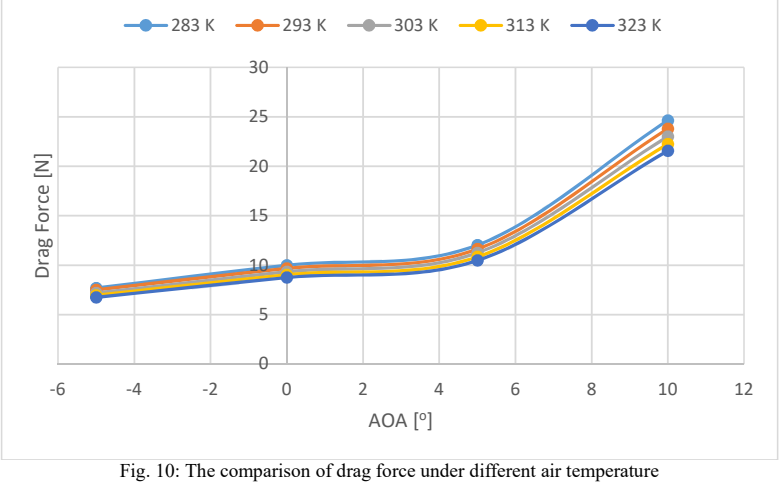

Fig. 10: The comparison of drag force under different air temperature

https://doi.org/10.5194/wes-2021-45
Preprint. Discussion started: 21 May 2021

eawe european academy of wind energy
Open Access WIND ENERGY SCIENCE DISCUSSIONS

3.6 Effect of Air Speed

RSM is used to investigate the effect of changing air speed on the airfoil characteristics. Both lift and drag coefficients are monitored at different air velocity. The velocities are (10, 20, 30, 37.5 and 50) m/s. Air temperature remains constant with a value of 293 K and turbulence intensity of 0.0011. Fig. 11 shows the comparison of lift coefficient under different air velocity. The lift coefficient increases with the increase of air velocity. The percentage in the increase of the lift coefficients at an angle of attack of 10º is more significant compared with the change of lift coefficient at lower angles of attack. There is a small change in the drag coefficients with the variation of air velocity as shown in fig. 12.

Fig. 13 shows the comparison of lift force under different air velocity. The lift force increases with the increase of air velocity. The rate of change at angle of attack of 10º is much considerable. It's about three times of that at 0º angle of attack. The increase in the lift force is proportional with the square of velocity so it preferable to operate the wind turbines at higher air velocity.

Fig. 14 shows the comparison of drag force under different air velocity. The drag force increases with the increase of air velocity.

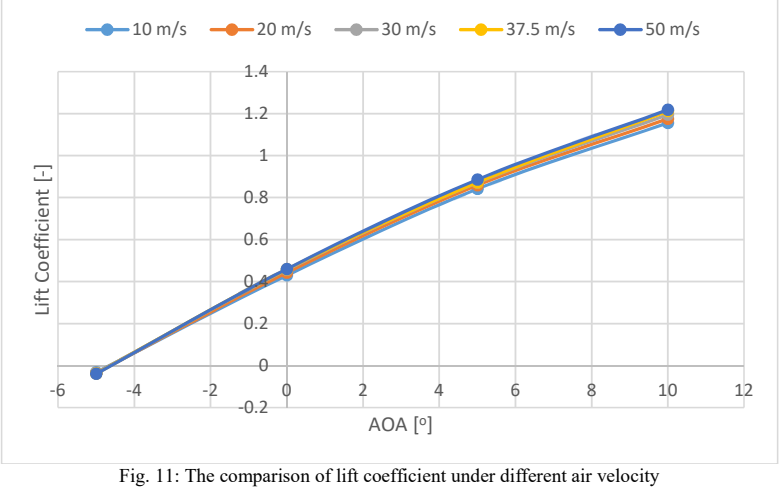

Fig. 11: The comparison of lift coefficient under different air velocity

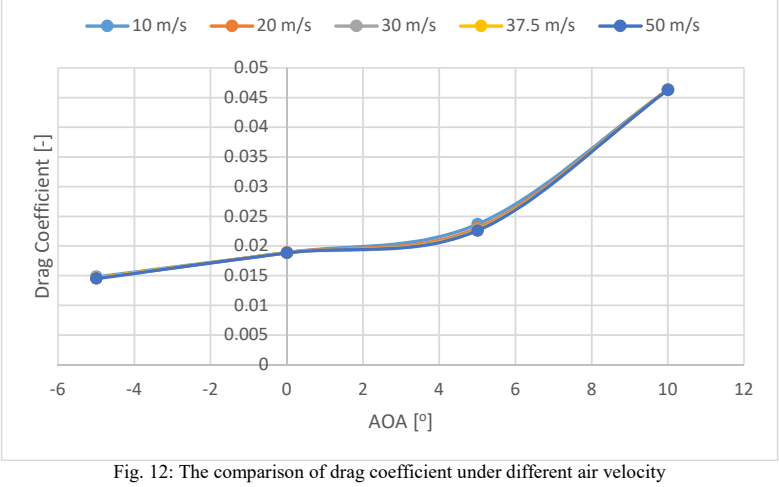

Fig. 12: The comparison of drag coefficient under different air velocity

https://doi.org/10.5194/wes-2021-45
Preprint. Discussion started: 21 May 2021

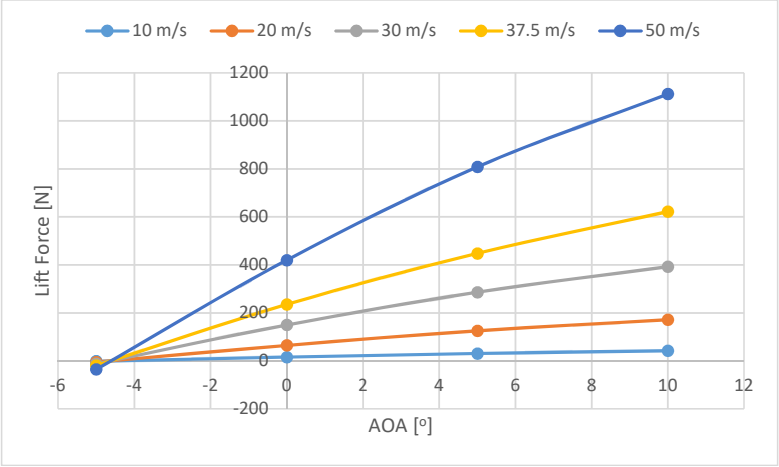

Fig. 13: The comparison of lift force under different air velocity

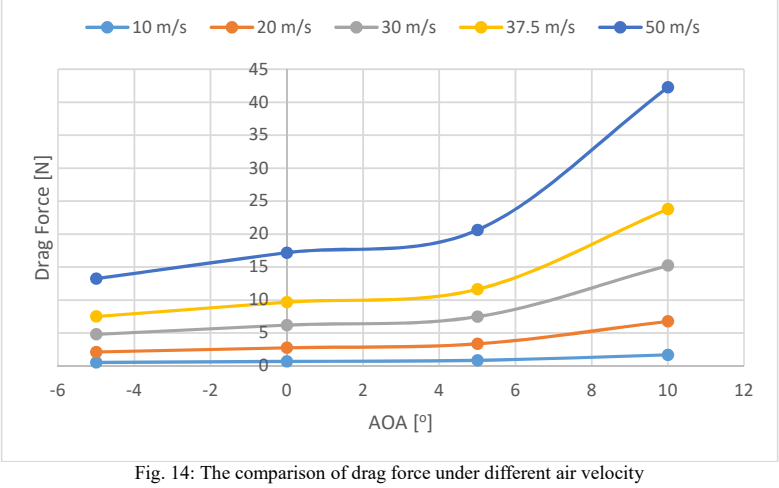

Fig. 14: The comparison of drag force under different air velocity

3.7 Effect of Turbulence Intensity

The effect of changing air flow turbulence intensity on the airfoil characteristics is investigated by simulate the airfoil with RSM as a turbulence model. Both lift and drag coefficients are monitored at different turbulence intensity of 0.0011, 0.1, 1, 10 and 20. Air velocity remains constant with a value of 37.5 m/s and temperature of 293 K. Fig. 15 shows the comparison of lift coefficient under different turbulence intensity. The lift coefficients are close to each other with a very small variation. The little change of the lift coefficient is in a direct relation with the turbulence intensity. Also, there was no noticeable change in the drag coefficients with the variation of air temperature as shown in fig. 16.

Fig. 17 shows the comparison of lift force under different turbulence intensity. The lift force does not change significantly with the change of the turbulence intensity.

Fig. 18 shows the comparison of drag force under different turbulence intensity. The drag force does not change significantly with the change of the turbulence intensity.

https://doi.org/10.5194/wes-2021-45
Preprint. Discussion started: 21 May 2021

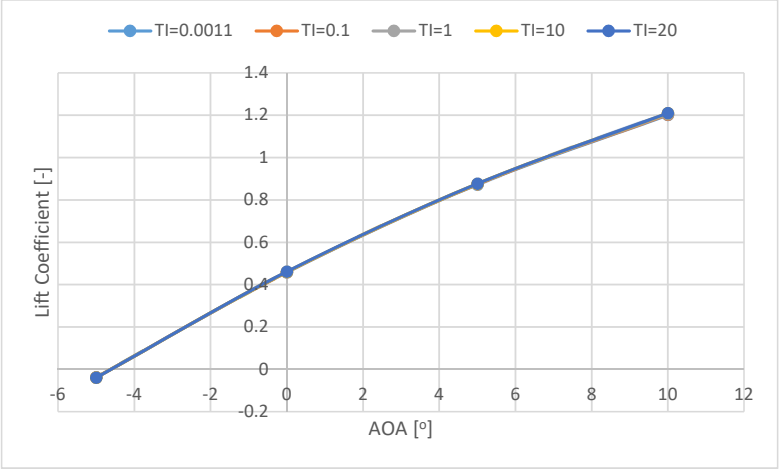

Fig. 15: The comparison of lift coefficient under different air turbulence intensity

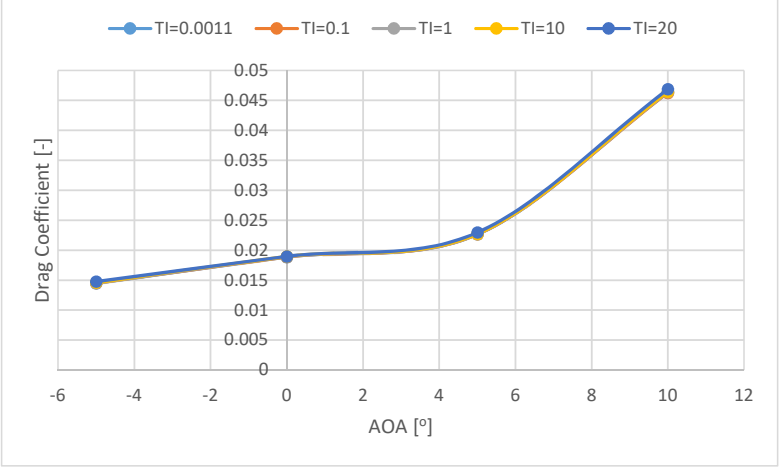

Fig. 16: The comparison of drag coefficient under different air turbulence intensity

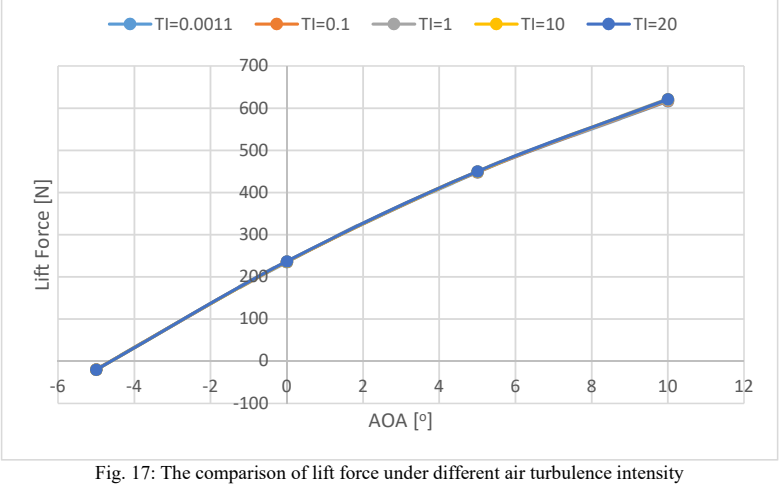

Fig. 17: The comparison of lift force under different air turbulence intensity

https://doi.org/10.5194/wes-2021-45
Preprint. Discussion started: 21 May 2021

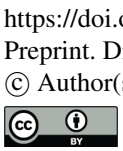

eawe european academy of wind energy
Open Access WIND ENERGY SCIENCE DISCUSSIONS

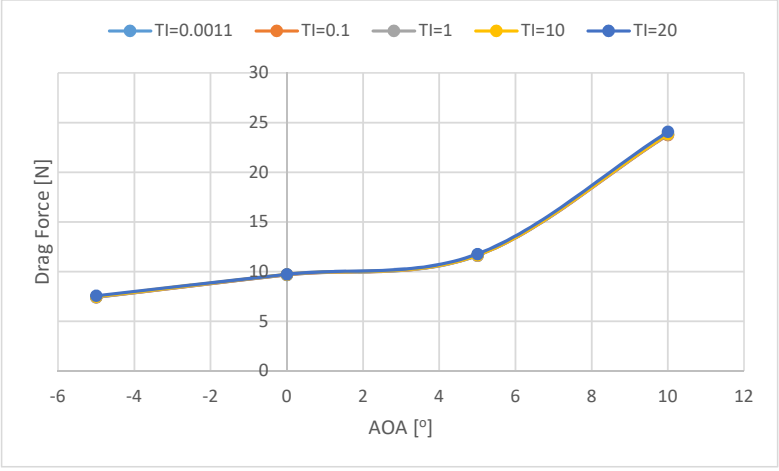

Fig. 18: The comparison of drag force under different air turbulence intensity

4 Conclusion

A numerical simulation study of the aerodynamic performance of DTU-LN221 airfoil is presented. The turbulence model has a definitely great influence on the numerical simulation results of wind turbine blade airfoil. Seven turbulence models are used to simulate the flow over the airfoil. These models are Inviscid, Spalart-Allmaras, k-ε, RNG k-ε, k-ω, SST k-ω and RSM. The lift and drag coefficients delivered from the simulation are compared with the wind tunnel experimental data. The range of the AOA of this simulation was between -10° to 20°. There was no a general model which can be called the best over the range of study. But RSM presented a good results over the other turbulence models especially in the range of AOA between -5° to 10°.

The RSM is selected to investigate the effect of changing AOA, air temperature, velocity and turbulence intensity on the characteristics of the airfoil. The following points can be concluded:

- By increasing the AOA (within the range of study - between -5° to 10°), the pressure in the lower side of the air foil increases while the velocity decreases.
- The larger attack angle, the greater difference of pressure coefficient between upper and lower surface.
- Even the change in lift and drag coefficients is very small with the variation of air temperature, there was a noticeable change in the lift and drag forces.
- The lift force decreases with the increase of air temperature.
- The lift coefficient increases with the increase of air velocity.
- The lift force increases rapidly with the increase of air velocity.
- The lift and drag forces does not change significantly with the change of the turbulence intensity.

Acknowledgements

The author extend their appreciation to the Deputyship for Research & Innovation, Ministry of Education in Saudi Arabia for funding this research work through the project number (DRI-KSU-1410)

References

Design of next generation wind turbine rotors (NextRotor), DTU Wind Energy, 2015a.
: FLUENT Ansys, Theory Guide Release 17, Ansys Inc.2015b.
: FLUENT Ansys, User's Guide Release 17, Ansys Inc.2015c.

https://doi.org/10.5194/wes-2021-45
Preprint. Discussion started: 21 May 2021

Allen, H. J. V., W.G.: Wall Interference in a Two-Dimensional FlowWind Tunnel, with Consideration of the effect of Compressibility, NACA Rep., 782, 155-184, 1944.
Allmaras, P. S. a. S.: A one-equation turbulence model for aerodynamic flows, Technical Report AIAA-92-0439. American Institute of Aeronautics and Astronautics, 1992.
B. E. Launder, G. J. R., and W. Rodi: Progress in the Development of a Reynolds-Stress Turbulence Closure, J. Fluid Mech., 68, 537-566, 1975.
Cheng, J., Zhu, W. J., Fischer, A., García, N., Madsen, J., Chen, J., and Shen, W. Z.: Design and validation of the high performance and low noise CQU-DTU-LN1 airfoils, Wind Energy, 17, 10.1002/we.1668, 2014.
Cheng, J. T. Z., W.J.; Fischer, A.; García, N.R.; Madsen, J.; Chen, J.; Shen, W.Z.: Design and validation of the high performance and low noise CQU-DTU-LN1 airfoils, Wind Energy, 17, 1817–1833, 2013.
G. H. Yu, X. C. Z., and Z. H. Du: Numerical simulation of a wind turbine airfoil: dynamic stall and comparison with experiments, Proc. IMechE., 224, 657-677, 10.1243/09576509JPE942, 2010.
Hao Wang, J. D., Bing Ma, Shuaibin Li: Aerodynamic simulation of wind turbine blade airfoil with different turbulence models, JVE INTERNATIONAL LTD. JOURNAL OF VIBROENGINEERING, 16, 2474-2483, August, 2014.
Hinze, J. O.: Turbulence, McGraw-Hill Publishing Co., New York1975.
Iñigo Aramendia , U. F.-G., , Ekaitz Zulueta, Aitor Saenz-Aguirre and Daniel Teso-Fz-Betoño: Parametric Study of a Gurney Flap Implementation in a DU91W(2)250 Airfoil, Energies, 12, 10.3390, 2019.
J., B.: Computational Fluid Dynamics: Principles and Applications, Third Edition., Elsevier Ltd., https://doi.org/10.1016/C2013-0-19038-1, 2015.
Ji Yaoa, W. Y., jianliang Wanga, Jianbin Xiec , Haipeng Zhoub , Mingjun Pengd, Yong Sund: Numerical simulation of aerodynamic performance for two dimensional wind turbine airfoils, International Conference on Advances in Computational Modeling and Simulation2012.
JT Cheng, W. Z., A Fischer, NR Garcia, J Madsen, J Chen, WZ Shen: Design and validation of the high performance and low noise CQU-DTU-LN1 airfoils, Wind Energy, 17, 1817-1833, 10.1002/we.1668, 2014.
Launder, B. E.: Second-Moment Closure: Present... and Future?, Inter. J. Heat Fluid Flow, 10, 282-300, 1989.
Launder, M. M. G. a. B. E.: Ground Effects on Pressure Fluctuations in the Atmospheric Boundary Layer, J. Fluid Mech., 86, 491-511, 1978.
Menter, F. R.: Two-Equation Eddy-Viscosity Turbulence Models for Engineering Applications, AIAA Journal, 32, 1598-1605, 1994.
Menter, F. R.: Review of the SST Turbulence Model Experience from an Industrial Perspective, International Journal of Computational Fluid Dynamics, 23, 2009.
N. Karthikeyan, K. K. M., S.Arun Kumar, S.Rajakumar: Review of aerodynamic developments on small horizontal axis wind turbine blade, Renewable and Sustainable Energy Reviews, 42, 801–822, 2015.
Namiranian, A.: 3D Simulation of a 5MW Wind Turbine, Mechanical Engineering, Bleckinge Institute of Technology, Karlskrona, Sweden, 72 pp., 2011.
ROHA. LSWT Campaign Report on DTU-C21; LM Internal Report: Jupitervej, D., 2012.,
Rosario Lanzafame, S. M., Michele Messina: 2D CFD Modeling of H-Darrieus Wind Turbines using a Transition Turbulence Model, 68th Conference of the Italian Thermal Machines Engineering Association, ATI2013, 45, 131-140, 2014.
S. A. Orszag, V. Y., W. S. Flannery, F. Boysan, D. Choudhury, J. Maruzewski, and B. Patel: Renormalization Group Modeling and Turbulence Simulations, International Conference on Near-Wall Turbulent Flows, Tempe, Arizona1993.
S. M. A. Aftab, A. S. M. R., N. A. Razak, K. A. Ahmad: Turbulence Model Selection for Low Reynolds Number Flows, PLoS ONE, 11, 15, 10.1371/journal.pone.0153755, 2016.
Schepers J. G., F. L., Rooij R. V., Bruining A.: Analysis of detailed aerodynamic field measurements using results from an aeroelastic code, Wind Energy, 7, 357-372, 2004.
Sessarego, M., Shen, W. Z., Sørensen, J. N., & Ramos García, N. : Design of Large Wind Turbines using Fluid-Structure Coupling Technique., Wind Energy, DTU, DTU Wind Energy, 2016.
Spalding, B. E. L. a. D. B.: Lectures in Mathematical Models of Turbulence, Academic Press, London, England1972.
W., V. H. K. a. M.: An introduction to computational fluid dynamics: the finite volume method, Pearson Education2007.
Wilcox, D. C.: Turbulence Modeling for CFD, DCW Industries, Inc. , La Canada, California1998.
Yang, J., Yang, H., Zhu, W., Li, N., and Yuan, Y.: Experimental Study on Aerodynamic Characteristics of a Gurney Flap on a Wind Turbine Airfoil under High Turbulent Flow Condition, Applied Sciences, 10, 7258, 2020.